ChemPubSoc Europe

DOI: 10.1002/slct.201802709

Chemistry SELECT Full Papers

Energy Technology & Environmental Science

Carbon-Enriched Cobalt Phosphide with Assorted Nanostructure as a Multifunctional Electrode for Energy Conversion and Storage Devices

Subramani Surendran,[a, c] Sathyanarayanan Shanmugapriya,[a] Yun Sung Lee,*[b] Uk Sim,*[c] and Ramakrishnan Kalai Selvan*[a]

A single-step hydrothermal technique is applied to prepare cobalt phosphide with multifarious nanostructures to signify its multifunctional capabilities. The prepared electrodes were intensely analysed for both the energy conversion and energy storage systems. The acquired Co–P with the assorted morphology of scaffolds and spherical of Co_2P/C electrode inspires with a significantly lower oxygen evolution reaction (OER) (271 mV(η_{10})) and hydrogen evolution reaction (HER) (207 mV(η_{10})) overpotentials to accelerate progressive electrocatalytic activity. Additionally, the energy storage capacity was revealed with the Co_2P electrode delivering an enriched specific capacity (322 C g^{-1} at 1 A g^{-1}) in conjunction with noteworthy rate capability (83%) and durable cycling stability (10000 cycles). Overall, an aqueous supercapattery device (Co_2P/C || AC) was fabricated providing superior energy density (35 Wh kg^{-1}) and an improved power density (5333 W kg^{-1}). The assembled water splitting system demanded a low cell voltage of 1.63 V to afford a high current density of 10 mA cm^{-2}. Moreover, the fabricated Co_2P/C || AC supercapattery coupled with the assembled water splitting system, to promote a supercapattery driven water splitting system profoundly proving the Co_2P propensity of handling the multifunctional challenges in terms of both storage and conversion aspects.

Introduction

It is well known that the cobalt-based compounds have been extensively used in various electrochemical and electrocatalytic applications especially supercapacitors, sodium-ion batteries, a zinc-air battery, water electrolyzers and fuel cells due to its appealing dualistic reversible redox couples and extreme strength in high alkaline electrolytes.[1–3] Among these, the cobalt phosphide has emerged itself as an impressive material than the oxides and sulphides.[3] Phosphides with its metalloid property combine with cobalt resembling a submetallic alloy, which possesses much higher intrinsic conductivity that induces bouncing kinetic rate overpowering the oxides. This empowers the fast electron transfer rate between the electrode and electrolyte that generates improved energy density in supercapacitors and upgraded catalytic activity for electrocatalysts.[4] Moreover, cobalt phosphide as an electrode appears to be more robust related to sulphide electrode due to its resilient durability in high alkaline electrolytes, whereas the sulphide based electrode has a tendency to decompose profoundly dropping its initial capacity. Hence, cobalt phosphides with its energetic reaction kinetics and robust strength are promptly reported as a favourable electrochemical and electrocatalysts material owing to its exceptional physicochemical properties, distinct metalloid characteristics, and astounding electrical conductivity.[5–7] In view of that, budding researchers are in high altitude to develop fine-tuned CoP based electrode materials by effective methods anticipated for various energy storage and conversion systems.

Conferring to conversion systems, CoP based electrode materials are employed predominantly as an effective electrocatalyst in the much-anticipated water splitting systems.[2,3] The water splitting system gives the impression to be a sensational renewable and clean energy resources to replace the use of limited fossil fuels.[8–10] The water splitting systems are strongly dependent on the oxygen evolution reaction (OER) and hydrogen evolution reaction (HER),[11,12] where the operational efficiencies of OER and HER reactions are explicitly dependent on their catalysts. Ruthenium or iridium-based noble metals are being used as effective electrocatalysts for OER and noble platinum-based electrodes are involved for HER catalysts.[13–15] The comparatively high cost, as well as the availability of these noble metals, confine the commercial capability of this application.[16] Therefore, identifying and exploiting noble metal-free electrocatalysts with upgraded catalytic activity is an operative way to reveal this system in large-scale applications.[17,18] Recently, Li et al. synthesised highly monodisperse CoP and Co_2P nanocrystals (NCs) for water electrolyzer and

[a] S. Surendran, S. Shanmugapriya, Dr. R. K. Selvan
Energy Storage and Conversion Devices Laboratory, Department of Physics, Bharathiar University, Coimbatore – 641–046, Tamil Nadu, India
E-mail: selvankram@buc.edu.in
[b] Prof. Y. S. Lee
Faculty of Applied Chemical Engineering, Chonnam National University, Gwangju 500–757, South Korea
E-mail: leeys@chonnam.ac.kr
[c] S. Surendran, Prof. U. Sim
Department of Materials Science & Engineering, Chonnam National University, Gwangju 61186, South Korea
E-mail: usim@jnu.ac.kr

Supporting information for this article is available on the WWW under https://doi.org/10.1002/slct.201802709

achieved a current density of 10 mA cm^{-2} at 1.56 V.[7] Similarly, Li et al. obtained the lower OER (250 mV at 10 mA cm^{-2}), and HER (239 mV at 20 mA cm^{-2}) overpotentials for the polycrystalline CoP/CoP_2 than the pure phase CoP.[19] Moreover, Cheng et al. synthesized a carbon cloth supported cobalt phosphide (CoP@CC) and obtained the lower overpotentials for HER (133 mV a current density of 10 mA cm^{-2}) and OER (300 mV a current density of 10 mA cm^{-2}) in an alkaline environment with satisfactory activity requesting 1.68 V to drive a current density of 10 mA cm^{-2} for water electrolyzer.[20] However, the above reported Co–P based electrocatalysts were prepared via two-step synthesis or high-temperature phosphorization method, which dwindles the large-scale commercialization of this CoP electrocatalysts. Therefore, considering the importance of CoP, this work reports the simplistic, single-step preparation method.

As of the energy conversion systems, the electrochemical capacitors or supercapacitors are considered as the promising energy storage device owing to its high power density with the rapid rate of charging and discharging, extended life, high safety, and sustainability.[21] Though delivering a high power density, the supercapacitors delivering low energy density that lures concerns over its commercial capabilities. In view of sorting out this deprivation, the conventional supercapacitors are hybridized and familiarized as a flexible supercapattery. The supercapattery devices are designed by a non-Faradaic electric double layer capacitor (EDLC)-type electrode as an anode (negative electrode) and the Faradaic -type electrode as a cathode (positive electrode).[22] Here, the customary highly conductive carbon-based materials such as activated carbon, 3D carbon nanostructures, porous carbon were used as EDLC electrodes to provide higher power density and the transition metal-based materials were employed as a battery-type electrode to ensure the enhanced energy density. In recent times, the Co–P based materials are much anticipated as a proficient battery-type electrode, which contributing high cycling stability, excellent rate capability, and ultimate energy density. So far, Cheng et al. synthesised the Co_2P hollow nanoflower structure and reported a high specific capacitance of 412.7 F g^{-1} at 1 A g^{-1}.[23] Likewise, Elshahawy et al. have grown CoP nanowires array on carbon cloth and reported the specific capacity of ~165.82 mAh g^{-1} at 1 A g^{-1} in 6 M KOH electrolyte.[24] Similarly, Zhang et al. have testified the synthesis of the mesoporous CoP nanowire arrays on carbon cloth and exhibited a high areal capacitance (1.89 F cm^{-2} at 3 mA cm^{-2}) and excellent cycling stability (~3% loss after the repetitive 4000 cycles at 18 mA cm^{-2}).[25] Also, Zheng et al. have fabricated solid-state asymmetric supercapacitor based on a CoP nanowire array as a negative electrode and MnO_2 nanowire array as a positive electrode, and a poly(vinyl alcohol) (PVA)/LiCl as a gel electrolyte.[26] Correspondingly, Chen et al. constructed a self-supported mesoporous Co_2P nanowire which delivered an excellent capacity (133 mAh g^{-1} at 1 A g^{-1}) and noticeable cycling life (5000 cycles).[27] Likewise, Zhang et al. assembled AC || CoP asymmetric supercapacitor, which delivered a high energy density (21.3 Wh kg^{-1}) and excellent stability (97.8%) for 5000 cycles.[28] Moreover, Chen et al. have synthesized one-dimensional (1D) Co_2P nanorods and 3D Co_2P nanoflowers by controlling the phosphating processes, where Co_2P nanorods and nanoflowers delivered a specific capacitance of 284 F g^{-1} and 461 F g^{-1} at 1 A g^{-1}, respectively. Furthermore, the fabricated asymmetric supercapacitor with graphene showed a high energy density of 24 Wh kg^{-1} at a power density of 0.3 kW kg^{-1}.[29]

However, most of the methods used to prepare Co–P comprises of multiple stages and high-temperature thermal treatment, which upsurges the construction cost that hurdles the large commercialization of the electrode material. Correspondingly, by implementing a different technique the size and morphology of the material can be altered, which can significantly improve the performance of the electrode material. Hence, trending a facile single-step approach to develop CoP electrodes can further initiate its role in various energy storage and conversion applications. Herein, we report a facile single-step hydrothermal technique is implemented to prepare the cobalt phosphide with multifarious nanostructures. The Co_2P electrode emboldens a superior OER (271 mV) and HER (207 mV) electrocatalytic activity. In addition, both the electrode expressed an enhanced energy storage capacity with a remarkable rate capability and resilient cycling stability. The fabricated aqueous supercapattery (Co_2P || AC) provided a superior energy density (35 Wh kg^{-1}) and an improved power density (5333 W kg^{-1}). The assembled water electrolyser system demanded a low cell voltage of 1.63 V to afford a high current density of 10 mA cm^{-2}. Thus, the Co_2P with all its superior electrode properties have profoundly proved its propensity of handling the multifunctional challenges in terms of both storage and conversion aspects.

Results and Discussion

Structural analysis

The phase purity and crystallinity of the prepared sample was characterized by the X-ray diffraction (XRD). The Co_2P sample was prepared using three different Co:P ratios (1:5, 1:10, 1:12) and the obtained diffraction patterns are given in Figure S1. All the XRD patterns perceived to be similar, where Co_2P prepared at 1:5 ratio shows strong high-intensity peaks when compared to the other conditions and well matches with the JCPDS card No. 98–009-4379. The prepared Co_2P is phase pure with an orthorhombic structure having the space group of P- nma (space group number 62) (Figure 1a). The lattice constants are calculated from the diffraction data using the CELREF software, which is found reliable with the standard lattice parameters (JCPDS card No. 98–009-4379). The obtained lattice constants are a = 5.6679 Å, b = 3.5027 Å, c = 6.6624 Å, and the cell volume is V = 132.26 × 10^6 pm^3. Similarly, using the Scherrer's formula, the calculated grain size of the Co_2P nanoparticles is ~27 nm.[30,31] Further, the obtained theoretical specific surface area is 29.75 m^2/g, which is calculated using equation 1[32,33]

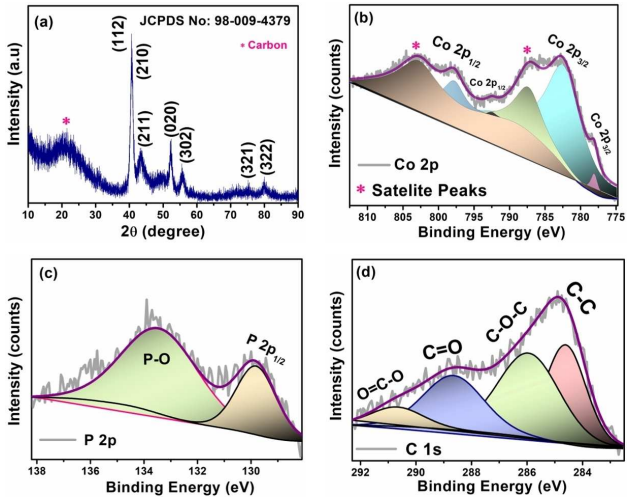

Figure 1. (a) XRD pattern and the deconvoluted XPS spectra of (b) Co (2p), (c) P (2p) and (d) C (1 s) of the prepared Co_2P nanostructure.

$$\text{Specific surface area} = \frac{6}{D \times \rho} \quad (1)$$

where the constant "6" represents the shape factor, D is the average particle size (in m) and ρ is the lattice density (in g/m^3). It can also be seen that the characteristic peak of carbon is observed around 20 to 30° in the XRD pattern (Fig. 1a), which clearly depicts the occurrence of carbon in the prepared Co_2P nanostructures. The existence of carbon in Co_2P can be endorsed to the inclusion of cobalt acetate as the starting precursor which serves as the only recognised source of the carbon. In order to validate the role of cobalt acetate for the formation of the carbon layer, cobalt nitrate was used as the cobalt source and the preferred hydrothermal synthesis procedure was carried out at different reaction conditions of 12, 24 and 48 h at two different temperatures like 180 and 200 °C. The obtained XRD patterns are shown in Figure S2&S3 (Supporting Information). The sample prepared at 180 °C under three different reaction periods (12, 24, 48 h) shows incomplete phase formation whereas the sample prepared at 200 °C (48 h) matches well with the standard JCPDS data (No: 98–009-4379) with some minor impurities. Further, one couldn't observe the presence of broad carbon peak around 20-30° as seen in Figure 1a. Hence, it can be concluded that the formation of carbon layer is obviously due to the procedure of employing cobalt acetate as Co precursor. Moreover, the presence of acetate also enhances the reaction rate by providing phase pure Co_2P structures at 180 °C which is only favourable at an augmented temperature of 200 °C with nitrate precursor. Hence the cobalt acetate being involved as a precursor for both carbon and Co for the formation of Co_2P/C nanostructures.

The XPS analysis opted for the better understanding of surface chemical composition and oxidation states of the constituent elements in the Co_2P/C sample. The comprehensive core level spectrum of Co (2p), P (2p) and C (1 s) are shown in Figure 1b-d. The peaks at 778.47 eV and 792.92 eV in the Co 2p core-level spectrum of Co_2P (Figure 1b), are endorsed to the Co $2p_{3/2}$ and Co $2p_{1/2}$ spin-orbital splitting of the cobalt species in cobalt phosphide.[34] Here, the peak at a binding energy of 778.47 eV is positively shifted from an elemental Co, which clearly evidences the partial positive charge of $Co^{\delta+}$ in Co–P compound.[35] Similarly, the peaks at 781.96 and 797.92 eV with their two corresponding satellite peaks (787.81 and 804.81 eV) in the Co 2p spectra are consistent with the Co $2p_{3/2}$ and Co $2p_{1/2}$ of the oxidized divalent (Co^{2+}) cobalt species.[26] Figure 1c shows the de-convoluted XPS spectrum of P 2p, where the peak at a binding energy of 129.87 eV corresponding to the P $2p_{1/2}$ of P in Co_2P, which was negatively shifted from the elemental P carries a partial negative charge of $P^{\delta-}$. Subsequently, a broad peak at 133.59 eV is ascribed to the oxidized P species due to the atmospheric contact of the sample.[29] Moreover, the existence of carbon was further acknowledged from the peaks of the XPS spectrum. The C 1s spectrum of carbon (Figure 1d) is de-convoluted into four prominent peaks at binding energies of 284.63, 285.99, 288.68, and 290.79 eV that can be attributed to the sp^2-hybridised C, sp^2-C bonded to O, C=O, and O=C-O, respectively.[36] The XPS result specifies that the evidential presence of P-bonded cobalt atoms in cobalt phosphide may provide electron transfer channels that enrich the conductivity of the prepared Co_2P. Similarly, the divalent cobalt species (Co^{2+}) may involve in the redox reactions of charge storage.[37] Further, the partial positive charge of Co and partial negative charge of P results in a transfer of electron density from Co to P, which could facilitate the adsorption and desorption of reactants and products, respectively during the electrocatalytic evolution reactions.[38]

Morphological Analysis

The FESEM image (Figure 2a) reveals the formation of scaffold-like Co_2P/C nanostructures, framed by uniformly embraced

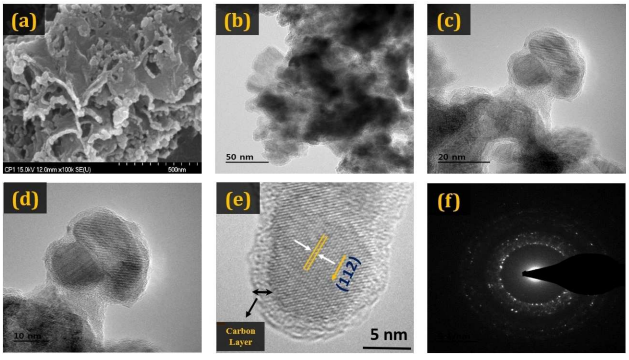

Figure 2. (a) FESEM, (b) TEM, (c-e) HRTEM and (f) SAED pattern of the prepared Co_2P nanostructures.

spherical nanoparticles. The developed spherical shape nanoparticles work as a frontier that associates several scaffolds to tailor a composed nanostructure. This kind of scaffold arrangements is well-thought-out to influence the electrochemical properties since the material gets well exposed to benefit

exchange reactions. Additionally, the existence of spherical nanoparticles in consort with the scaffold-like nanostructures promotes in crafting more number of active sites, because the morphology is framed in such a way to promote tunnel-like pathways.[39–41] These pathways extremely pave way for the increased accessibility of electrolyte into the concealed portions of the material which would obviously increase the number of active sites. Thus, it provisions the adsorption of an enormous number of ions during the electrochemical activity. The size of the individual spherical nanoparticle was calculated using Scion image software, which is around 45 nm. Also, tiny pore-like openings are seen which can further facilitate the transfer of ions to the depth of the electrode.

Similarly, the TEM image (Figure 2b) evidently depicts the scaffold-like nanostructures of Co_2P with a dark region, along with the frame of spherical particles. It also spectacles the porous nature of the material resembling the FESEM image. Figure 2 (c-e) reveals the HRTEM images of Co_2P/C with different magnification. Figure 2e shows the HRTEM image of Co_2P/C with distinct lattice fringes through interplanar distances of 0.22 nm, corresponding to the high intense (112) plane of the orthorhombic Co_2P crystal structure. It can also be seen that a thin layer of carbon (~2-3 nm) coated on the surface of the individual particles. The SAED pattern in Figure 2f elucidates the polycrystalline nature of the Co_2P/C nanostructures. Figure S4 (Supporting Information) shows the EDS spectrum of the respective Co_2P/C sample. The spectrum data reveals that in the prepared Co_2P/C, the Co element holds 47.09 at. %, P element owns 24.74 at. % and the carbon element relishes with the remaining 28.16 at. % explicating the mapped images.

Electrocatalytic properties of the Co_2P/C electrodes

Oxygen Evolution Reaction

The linear sweep voltammetry (LSV) curves of nanostructured Co_2P/C were examined to identify the OER activity in 1 M KOH electrolyte and compared with ruthenium oxide (RuO_2) and commercial carbon cloth (CC). Figure 3a depicts two distinct peaks witnessed initially at 1.1 and 1.4 V (vs RHE) owing to the oxidation reactions associated with the Co^{2+}/Co^{3+} and Co^{3+}/Co^{4+} redox couples.[42] The prepared scaffold-like Co_2P electrocatalyst associated with the spherical nanoparticles has shown an excellent catalytic activity than the auxiliary electrocatalysts (RuO_2 and CC) with an essential onset potential at 1.47 V (vs RHE). At this juncture, the possible oxygen gas bubbles were seen spawned out from the surface of the electrode. These gas bubbles on the surface of the electrode were expelled out by increasing the applied potential. The prepared Co_2P/C electrocatalyst requisite an overpotential of 298 mV to attain an elevated current density of 20 mA cm^{-2}, whereas the commercial RuO_2 electrocatalyst and CC required seemingly high overpotentials of 301 mV and 406 mV to attain the similar current density, respectively. The prepared Co_2P electrocatalyst offered a relatively enhanced OER activity compared to the other reported Co based electrodes, as listed in Table 1.[43–56]

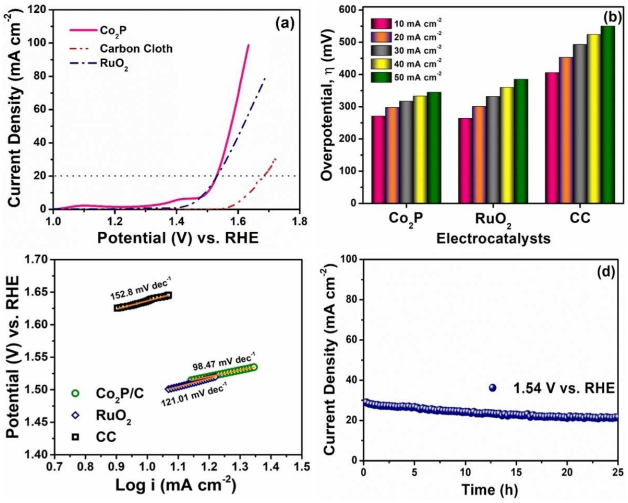

Figure 3. (a) LSV polarization curves for OER activity, (b) The necessary overpotential to achieve different current densities for different electrocatalysts, (c) Corresponding OER Tafel plots, and (d) Chronoamperometric curve of Co_2P.

Figure 3b illustrates the required OER overpotentials of different electrocatalysts to achieve augmented current densities (10 to 50 mA cm^{-2}). Initially, both the Co_2P and RuO_2 electrocatalysts were seen to dwell in identical curves at a current density of 10 mA cm^{-2} demanding equivalent overpotentials of 271 and 264 mV. As the potential increases, the Co_2P tends to move much straighter demanding low overpotentials of 298, 317, 333 and 345 mV at 20, 30, 40, and 50 mA cm^{-2} resulting in better catalytic activity. Whereas, the RuO_2 goes wider from the Co_2P curve yielding higher overpotentials (301, 332, 360 and 385 mV) at similar current densities confirming the enhanced OER catalytic activity of Co_2P.

The electrochemically active surface area (ECSA) remains to be the most important parameter to validate the intrinsic activity of the electrode materials. In general, the ECSA is estimated from the electrochemical double-layer capacitance, C_{dl} which is determined from the CV measurements obtained under non-Faradaic potential range where the current is solely contributed by the electrical double layer charging/discharging. In such potential range, the current contributed from the charge transfer during electrode reactions is almost negligible. Based on which, the CV curves were obtained in a potential range of 0.05 to 0.10 V versus Hg/HgO at different scan rates (Figure S5a (Supporting Information). The measured charging currents were plotted against the scan rates to obtain a linear fit deriving C_{dl} based on equation 2 (Figure S5b (Supporting Information).

$$i_c = \upsilon \times C_{dl} \quad (2)$$

where i_c and υ is the charging current and scan rate respectively. The C_{dl} of Co_2P/C electrocatalyst was calculated to

Table 1. Comparison of OER and HER performance in 1.0 M KOH with other non-noble-metal electrocatalysts.

Catalyst	Substrate	OER Overpotential [mV] @ 10 mA cm^{-2}	HER Overpotential [mV] @ 10 mA cm^{-2}	Ref.
2D porous oxygen incorporated CoP porous nanosheets	GCE	280	158	[43]
CoP/C	GCE	320		[44]
CoP/Cu foil	GCE	345		[45]
CoP	GCE	282		[46]
CoP/rGo	GCE	340	150	[47]
Co3O$_4$@C/CP	GCE	370		[48]
Co$_2$B-500	GCE	380	328	[49]
CoP@rGO	GCE	280		[50]
Co/CoP	GCE	340		[51]
CoP-mesoporous nanorod arrays	GCE	290		[52]
Oxygen doped CoFeP	GCE	274.5		[53]
CP/CTs/Co-S	GCE	306		[54]
Co–P@NC	GCE	370		[55]
CoP Hollow Polyhedron	GCE	400		[56]
Co$_2$P/C	CC	271	207	This work

be 0.1198 mF cm^{-2}. From the double-layer capacitance, the ECSA is calculated using the relation (3),

$$ECSA = C_{dl}/C_s \quad (3)$$

Where Cs is the capacitance of an atomically smooth surface area of the material per unit area obtained at identical electrolytic conditions which are around 0.04 mF cm^{-2} for 1 M KOH. Thus the ECSA of Co$_2$P/C was calculated to be 2.975 cm^{-2}. The obtained high ECSA of Co$_2$P/C electrocatalyst can be attributed to the presence of carbon along the metal phosphide since the carbon facilitates the electrical double layer capacitance at top-notch.

Moreover, the Tafel analysis is carried out to discuss the rate determining step involved in the oxygen evolution reaction and is presented in Figure 3c. The Tafel slope was obtained by fitting the Tafel curves of Co$_2$P, RuO$_2$ and CC, with the Tafel equation ($\eta = b \log j + a$). The rate determining step of Co$_2$P electrocatalyst was depicted to be a single-electron transfer step with a minimum Tafel slope of 98.47 mV dec^{-1}. In general, the cobalt-based non-oxide electrocatalysts are proposed to follow the possible OER catalytic mechanism in an alkaline medium as follows,[57]

$$Co + 2\,OH^- \rightarrow Co(OH)_2 + 2\,e^- \quad (4)$$

$$3\,Co(OH)_2 + 2\,OH^- \rightarrow Co_3O_4 + 4\,H_2O + 2\,e^- \quad (5)$$

$$Co_3O_4 + H_2O + OH^- \rightarrow 3\,CoOOH + e^- \quad (6)$$

$$CoOOH + OH^- \rightarrow CoO_2 + H_2O + e^- \quad (7)$$

Overall OER:

$$4\,OH^- \rightarrow 2\,H_2O + O_2 + 4\,e^- \quad (8)$$

Here, the catalytic mechanism of Co$_2$P is thus anticipated that the Co atoms on the surface of the prepared Co$_2$P electrode are partially surface oxidized to form the CoOOH active species that can hasten the oxidation of adsorbed OH$^-$ species into molecular oxygen. Subsequently, at higher potentials, the CoOOH get rather oxidized to CoO$_2$, an adsorbed intermediate phase over the Co$_2$P electrode that serves as the most favourable active species for OER.[57]

The chronoamperometry (CA) in Figure 3d were run at a constant potential of 1.54 V (vs RHE) for 25 hours. The unceasing evolution of O$_2$ bubbles from the electrode surface and the negligible changes in the current value throughout the completion of CA scrutiny ensure the highly stable nature of the prepared Co$_2$P electrocatalyst for OER activity. A slight degradation noted during the intermediate 10 to 20 hours session of the CA analysis was due to the chemical or structural degradation caused on the electrode-electrolyte interface.[58] This phenomenon resulted in a minute drop in the high reaction rate of the electrocatalyst, which later stabilizes itself over 25 hours, evidencing the sturdy nature of the electrocatalyst. The improved OER catalytic activity of the Co$_2$P sample can be ascribed to the electrochemically active transition metal Co in the phosphide. Moreover, the scaffold-like Co$_2$P nanostructures relish with the superior exposure of catalytically active sites on the surface that enhances the efficiency of the OER activity.[59,60]

Hydrogen Evolution Reaction

Similarly, the linear sweep voltammetry (LSV) curves of nanostructured Co$_2$P for HER activity was also examined compared to commercial platinum carbon electrocatalyst (Pt/C 10%) and commercial carbon cloth (CC) in 1 M KOH electrolyte. Figure 4a spectacles that the prepared scaffold-like Co$_2$P electrocatalyst associated with the spherical nanoparticles shown an excellent catalytic activity with an essential onset potential at 0.16 V (vs RHE). At this juncture, the possible hydrogen gas bubbles were seen spawned out on the surface of the electrode. These gas bubbles on the surface of the electrode were expelled out by

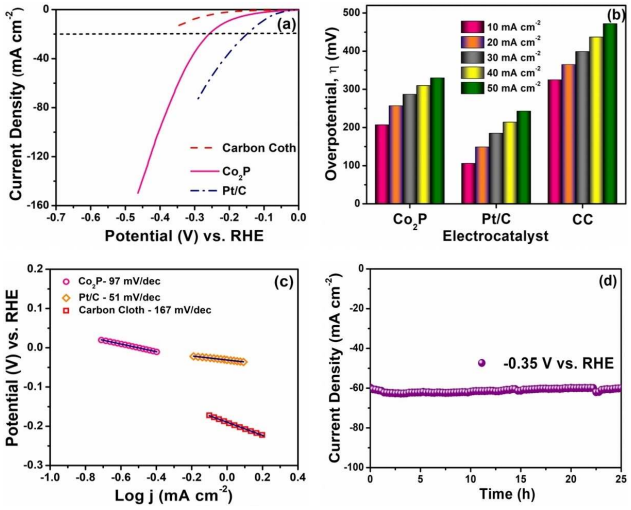

Figure 4. (a) LSV polarization curves for HER activity, (b) The necessary overpotential to achieve different current densities for different electrocatalysts, (c) Corresponding HER Tafel plots, and (d) Chronoamperometry of Co_2P/C.

increasing the applied potential. The prepared Co_2P electrocatalyst requisite an overpotential of 257 mV to attain an elevated current density of 20 mA cm^{-2}. Compared to the state of the art commercial Pt/C (149 mV) electrocatalyst, the Co_2P requisite a rationally equivalent overpotential to attain the similar current density. Moreover, the prepared Co_2P electrocatalyst offered a relatively enhanced HER activity compared to the other reported Co based electrodes, as listed in Table 1.[43,47,49]

Figure 4b illustrates the required HER overpotentials for different electrocatalysts to achieve augmented current densities (10 to 50 mA cm^{-2}). Though, the overpotential difference between the Pt/C and Co_2P is somewhat high in the beginning, as the potential increments the Co_2P tends to move squarer demanding low overpotentials of 207, 257, 287, 310 and 330 mV at an augmented current densities of 10, 20, 30, 40, and 50 mA cm^{-2} resulting in better catalytic activity. The HER Tafel analysis was carried out, and the obtained Tafel plots are exemplified in Figure 4c. Since the most promising reaction pathway of HER in an alkaline medium follow the Volmer–Heyrosky-Tafel mechanism that includes an initial step of hydrogen adsorption (b ≈ 120 mV/dec), followed by either electrochemical desorption (b ≈ 40 mV/dec) or a recombination reaction (b ≈ 30 mV/dec), the obtained low Tafel slope of 97 mV/ dec for Co_2P electrocatalyst transpires the rate-determining step as the discharge reaction. Because, in general, the hydrogen adsorption/discharge reaction is a kinetically sluggish phenomenon which indeed relies on water dissociation involving high energy barrier.[34] The CA analysis was studied (Figure 4d) for a constant potential of −0.35 V (vs RHE) for 25 hours, which illustrated a slight rise in the current rather than a drop elucidating the extraordinary strength of the Co_2P electrocatalyst. The uninterrupted evolution of gas bubbles from the surface of the electrode all through the CA analysis exemplifies the excellent electrocatalytic property of the Co_2P electrocatalyst.

Electrochemical properties of the Co_2P Electrode

To evaluate the electrochemical performance of the prepared Co_2P electrode, sequential electrochemical trials were carried out by a three-electrode system using 1 M KOH as the electrolyte.[22] Figure 5a represents the typical cyclic voltammetry (CV) curves of the Co_2P electrode at various scan rates from 1 to 10 mV s^{-1} with its potential ranging from 0 to 0.6 V (vs Hg/HgO). The CV curves show a pair of two prominent redox peaks unlike the standard rectangular curve of EDLCs, endorsing the battery-like behaviour of the Co_2P electrode.[21] The reversibility of the electrode can be adjudicated by the identical behaviour of the anodic and cathodic peaks. The two couples of redox peaks at 0.19/0.18 V and 0.52/0.50 V are embarked due to the characteristic oxidation of Co^{2+}/Co^{3+} to Co^{3+}/Co^{4+} state and likewise the reduction of Co^{4+}/Co^{3+} to Co^{3+}/Co^{2+} state, respectively.[61] The corresponding Faradaic electrochemical reaction involved as follows.[22]

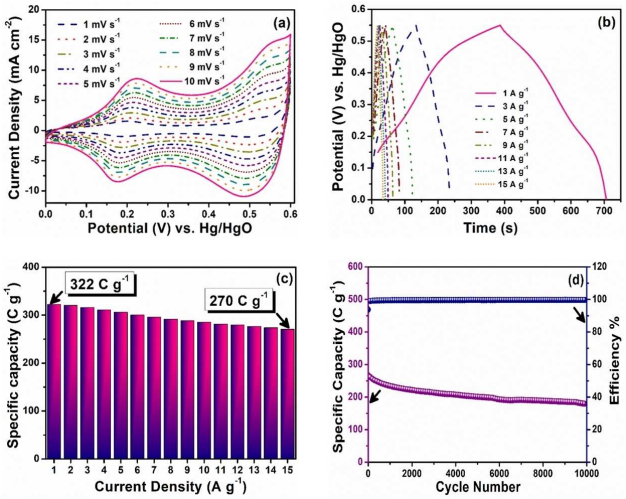

Figure 5. (a) CV curves of Co_2P/C with different scan rates, (b) GCD curves of Co_2P/C with different current densities, (c) Current density vs Specific capacity plot of Co_2P/C electrode, and (d) the cyclic stability curve of Co_2P/C along with its Coulombic efficiency.

$$Co_2P + 2OH^- \leftrightarrow Co_2P(OH^-)_2 + 2e^- \quad (9)$$

The area concealed by the CV curve corresponds to the energy storage capability of the Co_2P electrode. The broad cathodic and anodic peaks appear to stretch a huge volume of the current area in favour of the Co_2P electrode to deliver a high specific capacitance of 871 F g^{-1} at 1 mV s^{-1}. In Figure S6 (Supporting Information), both the anodic and cathodic peak current obtained from the CV curve increases with the square root of scan rate, which follows the Randles-Sevick equation yielding an adjacent R-square value of 0.998 and 0.997,

Table 2. Comparison of Co_2P electrode with other CoP electrodes.

Materials	Substrate Used	Electrolyte Used	Capacitance	Ref
Co_2P nanoshuttles	Nickel Foam (NF)	6 M KOH	246 F g^{-1} at 1 A g^{-1}	[5]
Hollow Co_2P nanoflowers	Nickel Foam (NF)	6 M KOH	412.7 F g^{-1} at 1 A g^{-1}	[23]
CoP/CC	Carbon Cloth binder free	6 M KOH	342. 8 F g^{-1} at 1 A g^{-1}	[24]
CoP	Carbon Cloth binder free	6 M KOH	1.89 F cm^{-2} at 3 mA cm^{-2}	[25]
CoP nanowire array	Carbon Cloth binder free	1 M LiCl	571.3 mF cm^{-2} at 1 mA cm^{-2}	[26]
Co_2P nanowire array	Nickel Fibre binder free	6 M KOH	133 mAh g^{-1} at 1 A g^{-1}	[27]
Co_2P nanoflowers	Nickel Foam (NF)	6 M KOH	416 F g^{-1} at 1 A g^{-1}	[28]
CoP nanosheet array	Carbon Cloth binder free	3 M KOH	645 F g^{-1} at 2 A g^{-1}	[37]
CoP	CC	1 M KOH	322 C g^{-1} at 1 A g^{-1} (586 F g^{-1} at 1 A g^{-1})	This work

respectively, revealing that the process is under a diffusion-controlled system.[62,63] The linearity achieved by the peak current values further justifies the redox behaviour of the Co_2P electrode, whereas the nonlinear curves reflect as the outcome of EDLC behaviour.

The galvanostatic charge-discharge (GCD) curves of the Co_2P electrode at diverse current densities between 1 and 15 A g^{-1} at a potential ranging from 0 to 0.55 V (vs Hg/HgO) is shown in Figure 5b. The obtained GCD curves display the formation of the plateau region authenticating the battery-like redox behaviour of the Co_2P electrode substantiated by the former CV curves. Legitimately, present-day reports suggest that it is inappropriate to relate the battery-type materials to the concept of capacitance due to the occurrence of Faradaic reactions in the alkaline aqueous electrolytes.[64–66] Hence, in accordance with the batteries, capacity (C g^{-1} or mA h g^{-1}) is the most appropriate and meaningful metric to be used for the battery-type materials. Therefore, the energy storage standards are conveyed in terms of capacity, which subsists virtual to the habitual term capacitance. As a result, the Co_2P electrode achieved a superior specific capacity of 322 C g^{-1} (586 F g^{-1} or 89 mAh g^{-1}) at a current density of 1 A g^{-1}. The accomplished extraordinary specific capacity of the Co_2P electrode surpasses the reported CoP based electrodes with a huge margin as tabulated in Table 2. The superior specific capacity of the Co_2P electrode can be endorsed to the multifarious morphology and the improved electronic conductivity of the material. Here, the multifarious morphology includes the scaffolds of Co_2P intends to expose the surface, which affords adequate room for the adsorption of additional ions from the electrolyte. The sphere-shaped particles with crooked surfaces existing contiguous to the scaffolds initiate more active sites on the surface of the electrode to affluence the superfluous addition of OH^- ions towards the electrode. In addition, the formation of unequal pores at the junctures permits the OH^- ions to penetrate from the surface into the indefinite depths of the electrode material refining more access for the OH^- ions addicted to the electrode. Moreover, the presence of carbon in the material boosts the electronic conductivity of the material to a greater extent to improve the reaction kinetics. Hence, the collective exertion of the prepared Co_2P electrode material has allured a colossal quantity of ions to get employed over the surface of the electrode, which has resulted in attaining superior capacity. Figure 5c displays the specific capacity retention of the prepared Co_2P electrodes from which it is clearly found that even at a high current density of 15 A g^{-1}, the Co_2P electrode has delivered a high specific capacity of 270 C g^{-1}, by upholding 83% of its initial specific capacity. Further, to investigate the succession rate of the Co_2P/C electrode, the cyclic stability tests were carried out for 10000 cycles at a static current density of 15 A g^{-1} in conjunction with 98% Coulombic efficiency (Figure 5d). Herein, as we expected the Co_2P electrode revealed a sturdy performance throughout the cycle with a negligible loss of its initial specific capacity. Figure S7 (Supporting Information), shows the EIS spectra of Co_2P fitted with an equivalent circuit to obtain the R_{ct} value. The Z-fit values obtained from the equivalent circuit are tabulated in Table S1. Figure S7 (Supporting Information) elucidates that the semi-circle of Co_2P is very much smaller with its diameter stretching around 0.9 Ω. The smaller semi-circle infers the large $1/R_{ct}$ value and enhanced conductivity of the prepared Co_2P that accounts the faster reaction kinetics of the electrode.[67,68] Therefore, with support from the impedance spectrum, high conductivity, faster kinetics and the surplus spongy nature of the Co_2P electrode have lured high specific capacity along with remarkable retention and cyclic stability compared to other Co_2P electrodes.

Electrochemical properties of fabricated (Co_2P/C || AC) supercapattery

Successful examination of Co_2P electrode has influenced to paradigm a supercapattery by separating prepared Co_2P electrode and activated carbon (AC) electrode with a separator bounded by an aqueous electrolyte medium and sealed.[22] The fabricated supercapattery was subjected by the CV and GCD techniques with an operating voltage from 0 to 1.6 V as shown in Figure 6 a&b. The specific capacitance/capacity of the device

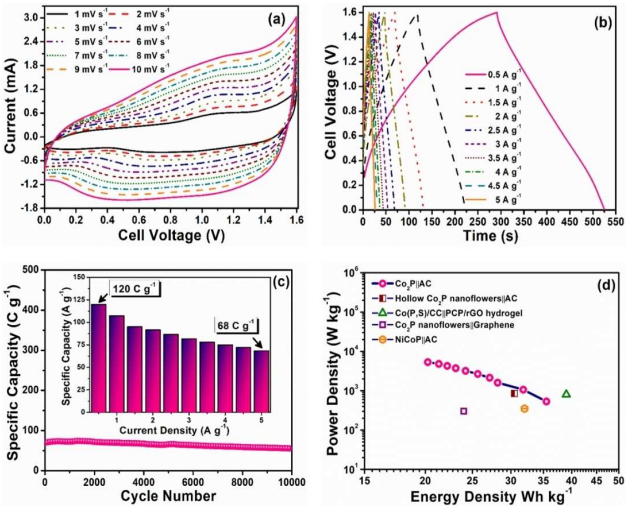

Figure 6. (a) CV curves of fabricated (Co_2P || AC) supercapattery with different scan rates, (b) GCD curves of the device at different current densities, (c) the cyclic stability curve of Co_2P/C, (inset) capacity retention plot and (d) Ragone plot of the fabricated (Co_2P || AC) supercapattery along with reported devices.

obtained from the CV and GCD curves are 254 F g^{-1} at 1 mV s^{-1} and 120 C g^{-1} at 0.5 A g^{-1}, correspondingly. From this analysis, an equivalent energy density of 35 and 20 Wh Kg^{-1} with respect to the power density of 533 and 5333 W Kg^{-1} was thrived by the designed device at a current density of 0.5 and 5 A g^{-1}, respectively. The cyclic stability of the fabricated device was analysed by performing charging and discharging trials for 10,000 cycles (as shown in Figure 6c). Figure S8 (Supporting Information) shows the impedance spectra obtained for the device fitted with an equivalent circuit to obtain the R_{ct} value. The Z-fit values obtained from the equivalent circuit are tabulated in Table S2. Figure S8 (Supporting Information) elucidates that the semi-circle of Co_2P is very much smaller yielding its R_s value around 2 Ω. The smaller semi-circle infers the large $1/R_{ct}$ value and enhanced conductivity of the device.[67,68] The Ragone plot in Figure 6d comprises in comparison of the prepared hybrid capacitor with reported hybrid Co_2P capacitors.

The reported hybrid Co_2P capacitors show a sufficient loss of its initial power density with respect to its increase in energy density. However, our device has grabbed immense control over it. Table 3 illustrates the comparison of the fabricated device with the reported Co_2P based capacitors. It elucidates in detail the disparities of the reported and the present work with respect to the used substrate, the concentration of the electrolyte, and the device performance. Scheme 1 displays the

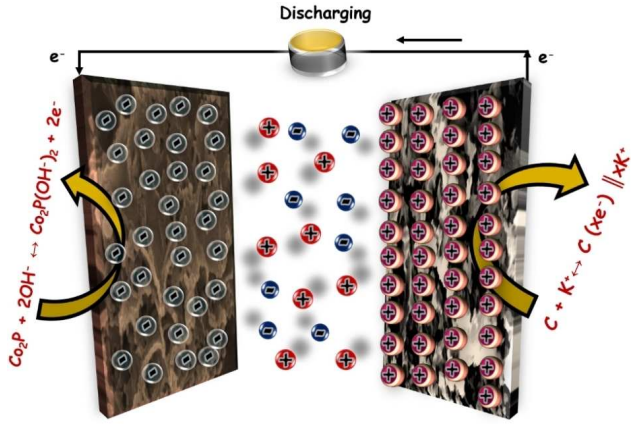

Scheme 1. The schematic illustration of the operational mechanism of the fabricated (Co_2P/C || AC) supercapattery.

schematic illustration of the operational mechanism of the device. When the potential is applied, the active Co species at

Table 3. Comparison of fabricated supercapattery with other CoP based capacitors.

Device Materials	Substrate Used	Electrolyte	Cell voltage	Specific Capacitance/ Capacity	Energy Density [Wh kg^{-1}]	Power Density [W kg^{-1}]	Ref. No.
Hollow Co_2P nanoflowers || AC	Nickel Foam (NF)	6 M KOH	1.7 V	75.9 F g^{-1} at 1 A g^{-1}	30.5 & 22.8	850 & 8500	[23]
Co(P,S)/CC || PCP/rGO hydrogel	Carbon Cloth binder free	6 M KOH	1.6 V	109.5 F g^{-1} at 1 A g^{-1}	39 & 18.7	800 & 30600	[24]
Co_2P nanoflowers || Graphene	Nickel Foam (NF)	6 M KOH	1.5 V	76.8 F g^{-1} at 0.4 A g^{-1}	24 & 8.8	300 & 6000	[29]
CoP@$Ni(OH)_2$ || AC	Carbon Cloth binder free	3 M KOH	1.8 V	220 F g^{-1} at 1 A g^{-1}	89.6 & 27.3	910 & 13400	[37]
NiCoP || AC	Nickel Foam (NF)	6 M KOH	1.6 V	164 C g^{-1} at 0.5 A g^{-1}	32 & 18	351 & 5586	[69]
Co_2P/C || AC	CC	1 M KOH	1.6 V	120 C g^{-1} at 0.5 A g^{-1}	35 & 20	533 & 5333	This Work

the cathode gets oxidised ($Co^{2+}/Co^{3+} \rightarrow Co^{3+}/Co^{4+}$) due to the accumulation of the negative (OH^-) on the surface. At the anode, the carbon electrode initiates charges separation (C (xe^-) || xK^+) by alluring the positive (K^+) ions on the surface forming an electric double layer. Owing to the highly porous nature of the Co_2P and AC electrodes, a number of ions get accommodated on the electrode surface and gets oxidised or attracted boosting the charge stored by the device. While discharging, the oxidised Co species at the cathode gets reduced, and the allured K^+ unleashed back into the electrolyte solution instigating the flow of electrons from the anode to cathode generating the power.. From the above results, it is familiar that the assembled Co_2P/C || AC device with the carbon cloth substrates has provided an enhanced performance when compared to other reported capacitor devices.

Lab Scale Water Electrolyser

As a result of the enriched multifunctional electrocatalytic and energy storage capability of the prepared Co_2P electrode, a lab-scale water electrolyser was designed as shown in Scheme 2.[7,49] The lab-scale water electrolyser was assembled

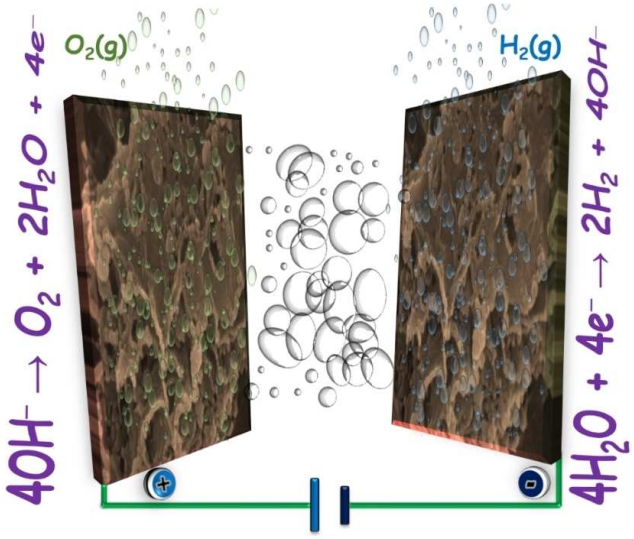

Scheme 2. The schematic illustration of the assembled lab-scale water electrolyzer.

by a two-electrode set up encompassing bifunctional Co_2P/C electrode as both anode and cathode. It is considered an archetype of the real-time application available in the market. The LSV curves of the water electrolyser are shown in Figure 7a. The assembled water electrolyser insists that a minimum potential of 1.63 V is necessary to attain a water-splitting current density of 10 mA cm^{-2}, resulting in the evolution of large troops of oxygen and hydrogen gas bubbles from both the surfaces of the electrodes. The CA analysis (Figure 7b) of the water electrolyser was completed at a static potential (1.75 V), and a steady state of evolution of gas was achieved for

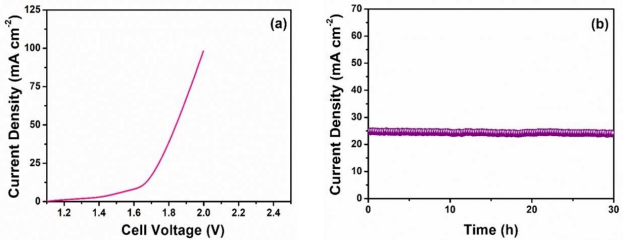

Figure 7. (a) LSV polarization curves of the device, (b) CA curves of the device for 30 hours

about 30 hours recalling the resilient strength of the Co_2P electrode. Henceforth, water electrolyser polarization of the Co_2P electrode was demonstrated with remarkably efficient catalytic activity, hasty kinetics and spirited strength during the study.

Thus, the Co_2P nanoparticles as a promising multifunctional electrode material were prepared by a single-pot hydrothermal method, with a unique assorted morphology. The Co_2P/C electrode has provided enhanced electrochemical performance as a supercapattery device and delivered a better electrocatalytic activity in terms of water electrolyser. The reported superior electroactivity of the prepared Co_2P/C electrode can be attributed to the following properties, (i) The prepared Co_2P is endowed with two kinds of cobalt elements with different combination ways. One being covalent bonded stores energy by Faraday reactions providing high capacitance while metal bonded cobalt atoms provide free electrons and enhance the electrical conductivity and rate capability.[37] (ii) Additionally, the existence of carbon also enriches the electrical conductivity of the material enhancing the electron transfer rate and reaction-kinetics during the electrochemical and electrocatalytic processes.[67,68] (iii) The HER catalytic nature of the Co_2P can be correlated with the unique charged natures of Co and P species. The small positive and negative charges on $Co^{\delta+}$ and $P^{\delta-}$ respectively has transformed it as hydride acceptor and proton acceptor sites in Co_2P to enhance the HER catalytic activity of the compound.[4] (iv) Furthermore, the unique assorted morphology has enhanced the accessibility of electrolyte and enables the incidence of bounteous ions on the electrode surface. Thus, the prepared Co_2P with modified unique morphology has profoundly performed well as a single electrode material for both electrochemical and electrocatalytic activity.

Conclusions

Here, a simplistic facile single-step hydrothermal technique is implemented to propose a cobalt phosphide with multifarious nanostructures. The prepared electrodes were keenly scrutinised through the basic electrochemical characterizations of both the energy conversion and energy storage systems. The Co_2P electrode emboldens a superior OER (271 mV) and HER (207 mV) electrocatalytic activity. In addition, both the electrode expressed an enhanced energy storage capacity with a

remarkable rate capability and resilient cycling stability. Overall, the aqueous supercapattery device (Co_2P/C || AC) was fabricated providing superior energy density (35 Wh kg^{-1}) and an improved power density (5333 W kg^{-1}). The assembled water electrolyser system demanded a low cell voltage of 1.63 V to afford a high current density of 10 mA cm^{-2}. The assembled water splitting device can be entangled with the fabricated supercapattery device to design a self-driven gadget. Thus, the Co_2P/C with all its superior electrode properties have profoundly proved its propensity of handling the multifunctional challenges in terms of both storage and conversion aspects.

Supporting Information Summary

The supporting information contains the details of experimental section, characterizations techniques used, electrode preparation, XRD patterns of Co_2P, EDS spectrum of Co_2P, Faradaic CV curves, double layer capacitance plot of Co_2P electrode, peak current (vs) scan rate plot of Co_2P electrode, Nyquist plots of Co_2P positive electrode and fabricated supercapattery device with corresponding Z-fit values and calculation formulas.

Acknowledgement

Prof.Y.S.Lee and Prof.Uk Sim greatly acknowledges to the National Research Foundation of Korea (NRF) grant funded by the Korea government (Ministry of Science, ICT & Future Planning) (2016R1 A4 A1012224, 2018R1 C1B6001267 and 2018R1 A5 A1025224), respectively.

Conflict of Interest

The authors declare no conflict of interest.

Keywords: Bifunctional electrocatalyst · Co_2P/C nanostructures · hydrogen evolution reaction · multifunctional electrode · oxygen evolution reaction · supercapattery · water splitting.

[1] M. Pramanik, S. Tominaka, Z. Wang, T. Takei, Y. Yamauchi, *Angew. Chem. Int. Ed.* **2017**, *56*, 1.
[2] L. Feng, H. Xue, *ChemElectroChem* **2017**, *4*, 20.
[3] J. Wang, Z. Liu, Y. Zheng, L. Cui, W. Yang, J. Liu, *J. Mater. Chem. A* **2017**, *5*, 22913.
[4] H. Li, S. Xu, H. Yan, L. Yang, S. Xu, *Small* **2018**, *14*, 1800367.
[5] F. Liang, L. Huang, L. Tian, J. Li, H. Zhang, S. Zhang, *CrystEngComm* **2018**, *20*, 2413.
[6] D. Zhou, L. Fan, *J. Mater. Chem. A* **2018**, *6*, 2139.
[7] H. Li, Q. Li, P. Wen, T. B. Williams, S. Adhikari, C. Dun, C. Lu, D. Itanze, L. Jiang, D. L. Carroll, G. L. Donati, P. M. Lundin, Y. Qiu, S. M. Geyer, *Adv. Mater.* **2018**, 1705796.
[8] C. Hu, L. Dai, *Adv. Mater.* **2017**, 1604942.
[9] F. Wang, X. Yang, B. Dong, X. Yu, H. Xue, L. Feng, *Electrochem. Commun.* **2018**, *92*, 33.
[10] Y. Wang, Z. Liu, H. Liu, N–T. Suen, X. Yu, L. Feng, *ChemSusChem* **2018**, *11*, 2724.
[11] V. S. Kale, U. Sim, J. Yang, K. Jin, S. I. Chae, W. J. Chang, A. K. Sinha, H. Ha, C. Hwang, J. An, H. Hong, Z. Lee, K. T. Nam, T. Hyeon, *Small* **2017**, *13*, 1603893.
[12] U. Sim, J. Moon, J. An, J. H. Kang, S. E. Jerng, J. Moon, S. Cho, B. H. Hong, K. T. Nam, *Energy Environ. Sci.* **2015**, *8*, 1329.
[13] A. Sivanantham, P. Ganesan, S. Shanmugam, *Adv. Funct. Mater.* **2016**, *26*, 4661.
[14] T. Tian, L. Huang, L. Ai, J. Jiang, *J. Mater. Chem. A* **2017**, *5*, 20985.
[15] C. Qiu, L. Ai, J. Jiang, *ACS Sustainable Chem. Eng.* **2018**, *6*, 4492.
[16] M. Wang, J. Jiang, L. Ai, *ACS Sustainable Chem. Eng.* **2018**, *6*, 6117.
[17] L. Ai, J. Su, M. Wang, J. Jiang, *ACS Sustainable Chem. Eng.* **2018**, *6*, 9912.
[18] J. Jiang, C. Zhang, L. Ai, *Electrochim. Acta* **2016**, *208*, 17.
[19] S. Li, G. Zhang, X. Tu, J. Li, *ChemElectroChem* **2018**, *5*, 701.
[20] Y. Cheng, F. Liao, W. Shen, L. Liu, B. Jiang, Y. Li, M. Shao, *Nanoscale* **2017**, *9*, 18977.
[21] S. T. Senthilkumar, R. K. Selvan, *ChemElectroChem* **2015**, *2*, 1111.
[22] B. Senthilkumar, Z. Khan, S. Park, K. Kim, H. Ko, Y. Kim, *J. Mater. Chem. A* **2015**, *3*, 21553.
[23] M. Cheng, H. Fan, Y. Xu, R. Wang, X. Zhang , *Nanoscale* **2017**, *9*, 14162.
[24] A. M. Elshahawy, C. Guan, X. Li, H. Zhang, Y. Hu, H. Wu, S. J. Pennycook, J. Wang, *Nano Energy* **2017**, *39*, 162.
[25] G. Zhanga, J. Fanga, L. Suna, S. Lib, K. Xuc, *Mater. Sci. Semicond. Process.* **2017**, *66*, 140.
[26] Z. Zheng, M. Retana, X. Hu, R. Luna, Y. H. Ikuhara, W. Zhou, *ACS Appl. Mater. Interfaces* **2017**, *9*, 16986.
[27] M. Chen, W. Zhou, M. Qi, J. Yin, X. Xia, Q. Chen, *J. Power Sources* **2017**, *342*, 964.
[28] G. Zhang, B. Li, M. C. Liu, S. Yuan, L. Niu, *J. Nanomaterials* **2017**, 9728591.
[29] X. Chen, M. Cheng, D. Chen, R. Wang, *ACS Appl. Mater. Interfaces* **2016**, *8*, 3892.
[30] K. V. Sankar, S. T. Senthilkumar, L. J. Berchmans, C. Sanjeeviraja, R. K. Selvan, *Appl. Surf. Sci.* **2012**, *259*, 624.
[31] T. Chengaiah, C. K. Jayasankar, K. Pavani, T. Sasikala, L. R. Moorthy, *Opt. Commun.* **2014**, *312*, 233.
[32] A. Shanmugavani, R.Kalai Selvan, *RSC Advances.* **2014**, *4,* 27022.
[33] V. D. Nithya, R. Kalai Selvan, K. Vediappan, S. Sharmila, C. W. Lee, *Appl. Surf. Sci.* **2012**, *261*, 515.
[34] K. Xu, H. Cheng, H. Lv, J. Wang, L. Liu, S. Liu, X. Wu, W. Chu, C. Wu, Y. Xie, *Adv. Mater.* **2018**, *30*, 1703322.
[35] J. Yu, Q. Li, Y. Li, C. Xu, L. Zhen, V. P. Dravid, J. Wu, *Adv. Funct. Mater.* **2016**, *26*, 7644.
[36] L. S. Sundar, G. O. Irurueta, E. V. Ramana, M. K. Singh, A. C. M. Sousa, *Case Studies in Thermal Engineering* **2016**, *7*, 66.
[37] J. Wen, S. Li, T. Chen, B. Li, L. Xiong, Y. Guo, G. Fang, *Electrochim. Acta* **2017**, *258*, 266.
[38] H. Lu, W. Fan, Y. Huang, T. Liu, *Nano Research* **2018**, *11*, 1274.
[39] A. N. Banerjee, V. C. Anitha, S. W. Joo, *Sci. Rep.* **2017**, *7*, 13227.
[40] S. Bosi, R. Rauti, J. Laishram, A. Turco, D. Lonardoni, T. Nieus, M. Prato, D. Scaini, L. Ballerini, *Sci. Rep.* **2015**, *5*, 9562.
[41] M. Sharma, G. I. N. Waterhouse, S. W. C. Loader, S. Garga, D. Svirskis, *Int. J. Pharm.* **2013**, *443*, 163.
[42] A. Sivanantham, P. Ganesan, L. Estevez, B. P. McGrail, R. K. Motkuri, S. Shanmugam, *Adv. Energy Mater.* **2018**, *8*, 1702838.
[43] G. Anandhababu, Y. Huang, D. D. Babu, M. Wu, Y. Wang, *Adv. Funct. Mater.* **2018**, 1706120.
[44] J. Chang, Y. Xiao, M. Xiao, J. Ge, C. Liu, W. Xing, *ACS Catal.* **2015**, *5*, 6874.
[45] N. Jiang, B. You, M. Sheng, Y. Sun, *Angew. Chem. Int. Ed.* **2015**, *54*, 6251.
[46] P. Wang, F. Song, R. Amal, Y. H. Ng, X. Hu, *ChemSusChem* **2016**, *9*, 472.
[47] L. Jiao, Y. Zhou, H. Jiang, *Chem. Sci.* **2016**, *7*, 1690.
[48] X. Yang, H. Li, A. Lu, S. Min, Z. Idriss, M. Hedhili, K. Huang, H. Idriss, L. Li, *Nano Energy* **2016**, *25*, 42.
[49] J. Masa, P. Weide, D. Peeters, I. Sinev, W. Xia, Z. Sun, C. Somsen, M. Muhler, W. Schuhmann, *Adv. Energy Mater.* **2016**, *6*, 1502313.
[50] G. Zhang, G. Wang, Y. Liu, H. Liu, J. Qu, J. Li, *J. Am. Chem. Soc.* **2016**,*138*,14686.
[51] Z. Xue, H. Su, Q. Yu, B. Zhang, H. Wang, X. Li, J. Chen, *Adv. Energy Mater.* **2017**, *7*, 1602355.
[52] Y. Zhu, Y. Liu, T. Ren, Z. Yuan, *Adv. Funct. Mater.* **2015**, *25*, 7337.
[53] J. Duan, S. Chen, A. Vasileff, S. Z. Qiao, *ACS Nano* **2016**, *10*, 8738.
[54] X. Zhang, J. Wang, H. Zhong, Z. Wang, F. Meng, *ACS Nano* **2016**,*10*,2342.
[55] M. Zhai, F. Wang, H. Du, *ACS Appl. Mater. Interfaces* **2017**, *9*, 40171.
[56] M. Liu, J. Li, *ACS Appl. Mater. Interfaces* **2016**, *8*, 2158.
[57] P. Chen, K. Xu, Z. Fang, Y. Tong, J. Wu, X. Lu, X. Peng, H. Ding, C. Wu, Y. Xie, *Angew. Chem. Int. Ed.* **2015**, *54*, 14710.

[58] D. S. Bick, T. B. Krebs, D. Kleimaier, A. F. Zurhelle, G. Staikov, R. Waser, I. Valov, *Langmuir* **2018**, *34*, 1347.
[59] X. Wang, R. Tong, Y. Wang, H. Tao, Z. Zhang, H. Wang, *ACS Appl. Mater. Interfaces* **2016**, *8*, 34270.
[60] Y. Bai, H. Zhang, L. Liu, H. Xu, Y. Wang, *Chem. Eur. J.* **2016**, *22*, 1021.
[61] K. V. Sankar, S. C. Lee, Y. Seo, C. Ray, S. Liu, A. Kundu, S. C. Jun, *J. Power Sources* **2018**, *373*, 211.
[62] J. Liu, J. Wang, Z. Ku, H. Wang, S. Chen, L. Zhang, J. Lin, Z. X. Shen, *ACS Nano* **2016**, *10*, 1007.
[63] J. Liu, M. Chen, L. Zhang, J. Jiang, J. Yan, Y. Huang, J. Lin, H. J. Fan, Z. X. Shen, *Nano Lett.* **2014**, *14*, 7180.
[64] P. Simon, Y. Gogotsi, B. Dunn, *Science* **2014**, *343*, 1210.
[65] Y. Gogosti, P. Simon, *Science* **2011**, *334*, 917.
[66] Y. Gogosti, *ACS Nano* **2014**, *8*, 5369.
[67] G. K. Veerasubramani, Y. Subramanian, M.-S. Park, G. Nagaraju, B. Senthilkumar, Y.-S. Lee, D.-W. Kim, *J. Mater. Chem. A* 2018, 6, 20056.
[68] S. Manoharan, S. Sahoo, P. Pazhamalai, S. J. Kim, *Int. J. Hydrogen Energy* 2018, 43, 1667.
[69] Y. Hu, M. Liu, Y. Hu, Q. Yang, L. Kong, L. Kang, *Electrochim. Acta* **2016**, *215*, 114.

Submitted: August 29, 2018
Accepted: November 8, 2018